

Accepted for Publication in the Astrophysical Journal

# Spatially Extended Brackett Gamma Emission in the Environments of Young Stars<sup>1</sup>

Tracy L. Beck

*Space Telescope Science Institute, 3700 San Martin Dr., Baltimore, MD 21218*

tbeck@stsci.edu

Jeffery S. Bary

*Colgate University, Department of Physics & Astronomy, 13 Oak Drive, Hamilton, NY 13346*

jbary@colgate.edu

and

Peter J. McGregor

*Research School of Astronomy & Astrophysics, Australian National University, Cotter Road, Weston, ACT 2611, Australia*

peter@mso.anu.edu.au

## ABSTRACT

The majority of atomic hydrogen Br $\gamma$  emission detected in the spectra of young stellar objects (YSOs) is believed to arise from the recombination regions associated with the magnetospheric accretion of circumstellar disk material onto the forming star. In this paper, we present the results of a K-band IFU spectroscopic study of Br $\gamma$  emission in eight young protostars: CW Tau, DG Tau, Haro

---

<sup>1</sup>Based on observations obtained at the Gemini Observatory, which is operated by the Association of Universities for Research in Astronomy, Inc., under a cooperative agreement with the NSF on behalf of the Gemini partnership: the National Science Foundation (United States), the Particle Physics and Astronomy Research Council (United Kingdom), the National Research Council (Canada), CONICYT (Chile), the Australian Research Council (Australia), CNPq (Brazil), and CONICET (Argentina).

6-10, HL Tau, HV Tau C, RW Aur, T Tau and XZ Tau. We spatially resolve Br $\gamma$  emission structures in half of these young stars and find that most of the extended emission is consistent with the location and velocities of the known Herbig-Haro flows associated with these systems. At some velocities through the Br $\gamma$  line profile, the spatially extended emission comprises 20% or more of the integrated flux in that spectral channel. However, the total spatially extended Br $\gamma$  is typically less than  $\sim 10\%$  of the flux integrated over the full emission profile. For DG Tau and Haro 6-10 S, we estimate the mass outflow rate using simple assumptions about the hydrogen emission region, and compare this to the derived mass accretion rate. We detect extended Br $\gamma$  in the vicinity of the more obscured targets in our sample and conclude that spatially extended Br $\gamma$  emission may exist toward other stars, but unattenuated photospheric flux probably limits its detectability.

*Subject headings:* stars: pre-main sequence — stars: winds, outflows — stars: formation — stars: individual (CW Tau, DG Tau, Haro 6-10, HL Tau, HV Tau C, RW Aur, T Tau, XZ Tau)

## 1. Introduction

H I emission lines are one of the defining characteristics of the classification of pre-main-sequence Sun-like sources known as T Tauri stars (TTS). Still in the midst of formation, the less evolved TTS, known as classical TTS (cTTS), are surrounded by optically thick disks of gas and dust. In most cases, these young pre-main-sequence stars are still interacting with and accreting matter from the innermost regions of their disks via stellar magnetic fields. In this magnetospheric accretion paradigm, the stellar magnetosphere guides disk material from the inner disk onto the stellar surface through magnetic channels. The gas travels along these channels or so-called accretion columns near free-fall velocities, terminating in an accretion shock at the stellar surface. It is generally accepted that the gas is heated and ionized prior to and after reaching the stellar surface and that the characteristic H I emission lines result, in part, from recombining and accreting hydrogen gas confined to these magnetic channels (Lynden-Bell & Pringle 1974; Uchida & Shibata 1984; Bertout et al. 1988).

Balmer H $\alpha$  emission is the dominant H I feature present in the optical spectra of cTTS, and the emission line strength (or line width) is often invoked as a measure of accretion rates for these sources (Muzerolle et al. 1998a). Spatially resolved observations of H $\alpha$  emission lines in these young stellar objects (YSOs) also show it to be a strong component of the optical line emission from outflows, indicating that the underlying stimulation mechanisms for the H I lines is likely to be a combination of phenomena. Magnetospheric accretion models

can successfully reproduce many aspects of the H I emission features detected in the spectra of young stars. However, they notably fail to account for the highest velocity gas in the H I line wings (Muzerolle et al. 1998a). Spectro-astrometric observations of the Pa $\beta$  emission feature in the cTTS DG Tau show that the high velocity blue-shifted gas ( $v > -200$  km s $^{-1}$ ) is extended in the same direction as [Fe II] at 1.644  $\mu$ m, a forbidden emission line feature that traces the known outflow in the DG Tau system. This illustrates why a model producing H I emission from accretion funnels does not account for high velocity gas forming the H I line wings (Whelan et al. 2004). While the high velocity gas is spatially shifted by as much as 0."5 around DG Tau (or  $\sim 70$  AU at the distance of Taurus-Auriga), the majority of the Pa $\beta$  emission remains coincident with the source. Although these results demonstrate that there are multiple processes for stimulating H I emission lines, the bulk of the emitting gas does seem to arise from radii within 14 AU of the central source constraining the emission to the magnetospheric accretion columns, inner gaseous disk, and the base of disk winds and outflows.

In the infrared, Br $\gamma$  (2.16  $\mu$ m) emission serves as a surrogate for H $\alpha$  as a signpost for circumstellar disk accretion in TTS (Najita et al. 1996). Br $\gamma$  line luminosities appear to correlate with mass accretion luminosity in brown dwarfs, cTTS, and Herbig Ae/Be stars (HAEBEs; Muzerolle et al. 1998a; Natta et al. 2004; Mohanty et al. 2003, 2005). Moreover, Br $\gamma$  and other lines in the infrared are less affected by optical depth effects that have proven problematic for using Balmer series lines to infer temperatures, densities, and geometries of the emitting gas. Historically, the problem of predicting the spectra emerging from a recombining hydrogen gas has been divided into two distinct cases, A and B (Baker & Menzel 1938). Case A theory applies to very low density gases that are optically thin to all transitions of the hydrogen atom, including the ultraviolet photons associated with the Lyman series transitions. Case B theory, which applies to higher density gases which are optically thick to UV photons but optically thin to all  $n \geq 2$  transitions, is often applied to the environments of T Tauri stars. In a Case B model of a recombining atomic hydrogen gas, Br $\gamma$  is  $\sim 0.8$ -1% of the flux of H $\alpha$  for a wide range of densities and temperatures ( $10^2 < n_e < 10^6$  cm $^{-3}$ ,  $5000\text{K} < T < 20000\text{K}$ ). H $\alpha$  is known to be a strong component in optical line emission from YSO outflows (Najita et al. 1996), it seems natural that a corresponding component of the Br $\gamma$  emission would also arise from the outflows. Yet, to date, there has been little evidence in the literature for spatially resolved Br $\gamma$  emission in the vicinity of YSOs, and hence nearly all Br $\gamma$  emission is assumed to arise from magnetospheric processes within the inner accretion zone. In fact, infrared interferometric observations of HAeBe stars reveal that the Br $\gamma$  often arises from very compact locations within the dust sublimation radius of the circumstellar disk (Eisner et al. 2009; Kraus et al. 2008). Though, a small extended Br $\gamma$  emission component can not be ruled out based on these observations. Further interferomet-

ric and spectro-astrometric programs that seek to reveal the inner  $\sim 1$  AU environments show that the compact  $\text{Br}\gamma$  is not always well modeled by disk emission alone (Eisner et al. 2010; Malbet et al. 2010). The analysis implies that a non-negligible component from outflowing gas needs to be incorporated into the models to explain the  $\text{Br}\gamma$  emission structure.

As an extension of the spectro-astrometric and interferometric studies mentioned above, imaging spectroscopy of these TTS can provide us with considerable insight into the geometric distribution of H I emitting gas in accreting systems. Three-Dimensional imaging spectroscopy techniques can help to disentangle the respective contributions to the H I emission features. With just one pointing of a telescope, imaging spectroscopy with integral field units (IFUs) can provide three-dimensional  $x, y, \lambda$  datacubes at high spatial resolution with simultaneous coverage of many emission lines of interest. There has recently been an increase in the capabilities for adaptive optics (AO) fed near IR integral field spectroscopy at 8-10 meter class observatories (Eisenhauer et al. 2000; McGregor et al. 2003; Larkin et al. 2006). IFUs optimized for AO spectroscopy have the power to spatially resolve emission line structures with less than  $0.''1$  extents over the full wavelength ranges sampled by typical IR spectrographs. As such, the new generation of IFUs provides the means to study the accretion and outflow environments in cTTSs.

In this paper, we present detections of spatially resolved  $\text{Br}\gamma$  emission in YSO environments from data acquired using the Near IR Integral Field Spectrograph at the Gemini North Observatory. We report on  $\text{Br}\gamma$  arising from eight classical TTS systems, and particularly highlight the spatially extended emission detected in four of these: DG Tau, Haro 6-10 (also known as GV Tau), HL Tau and HV Tau C.

## 2. Observations

Observations of the eight CTTSs listed in Table 1 were obtained using the Near IR Integral Field Spectrograph (NIFS) at the Frederick C. Gillette Gemini North Telescope on Mauna Kea, Hawaii. NIFS is an image slicing IFU fed by Gemini’s Near IR adaptive optics system, Altair, that is used to obtain integral field spectroscopy at spatial resolutions of  $\leq 0.''1$  with a spectral resolving power of  $R \sim 5300$  at  $2.2 \mu\text{m}$  (as measured from arc and sky lines; McGregor et al. 2003). The NIFS field has a spatial extent of  $3'' \times 3''$ , and the individual IFU pixels are  $0.''1 \times 0.''04$  on the sky. Data were obtained at the standard K-band wavelength setting for a spectral range of  $2.003\text{--}2.447 \mu\text{m}$ . All observations were acquired in natural seeing of better than  $0.''7$  for excellent AO correction.

The data sets for this study were acquired for commissioning and system verification

of NIFS in October 2005 and February 2006, GTO time in December 2006, and in queue mode in February 2007 (see Table 1). For each observation, a standard set of calibrations were acquired using the Gemini facility calibration unit, GCAL. The raw IFU frames were reduced into datacubes using the NIFS tasks in the Gemini IRAF package<sup>1</sup>.

Beck et al. (2008) discuss these NIFS data on DG Tau, HL Tau, HV Tau C, RW Aur, T Tau and XZ Tau in the context of spatially resolved molecular hydrogen emission lines. Hence the observational details, calibration, and data reduction information is described in great detail in that paper and excluded here. To study the Br $\gamma$  emission in the young stars, the absorption features from the A0 stellar type telluric calibration stars were removed by fitting and dividing Voigt absorption profiles in the 2.16  $\mu\text{m}$  spectral region and cleaning the calibration spectra for any small residuals. Observations of Haro 6-10 were acquired with the laser-fed AO system using the R $\sim$ 16.5 mag southern component in this 1."2 binary as the laser tip-tilt reference star. These data were obtained in excellent laser-quality weather, photometric with better than 0."5 seeing. The CW Tau and Haro 6-10 data were processed in a similar manner to all other data, as described above and in Beck et al. (2008). All or part of the data for each source in this project was observed during photometric conditions and were flux calibrated using K-band magnitudes estimated by comparison to the brightness of the A0 standard star used for telluric correction. With the exception of Haro 6-10, the derived fluxes of the systems (combined in the case of multiples) were within 10-15% of published or 2MASS magnitudes. For Haro 6-10, the NIFS IFU spectra were compared to infrared K-band images acquired nearby in time for a complimentary project, the difference in flux was less than 0.2 magnitudes between the two observations. We estimate that our overall data flux calibration is good to  $\pm$ 10-15%. The data cubes were interpolated onto a square pixel grid with 0."05 spatial sampling, and the velocity channel steps through the IFU cubes are  $\sim$ 29 km s $^{-1}$  pixels in extent at 2.20  $\mu\text{m}$  ( $\sim$ 56 km s $^{-1}$  2 pixel resolution). The final reduced, combined, telluric corrected, and flux-calibrated datacubes of the Br $\gamma$  line emission for each target are discussed in detail in the following sections.

### 3. Spatially Extended Br $\gamma$ Emission from YSO Environments

The data acquired for this project, described in detail in the preceding section, were obtained with the goal of studying the K-band features of molecular hydrogen emission. The IFU spectral data were discussed by Beck et al. (2008) in this context. We never expected to detect spatially extended Br $\gamma$  emission in any CTTS. This was a serendipitous discovery,

---

<sup>1</sup>Information on the Gemini IRAF package is available at <http://www.gemini.edu/sciops/data/dataIRAFIndex.html>

revealed as we stepped through the raw velocity cube at  $\text{Br}\gamma$  wavelengths in the Haro 6-10 S data. The clear detection of spatially extended emission from the Haro 6-10 S jet prompted us to take a closer look at the  $\text{Br}\gamma$  emission in all TTS for which K-band IFU spectra had been obtained. As presented and discussed in the following, we have found significant spatially extended  $\text{Br}\gamma$  emission in four of the eight stars presented here: DG Tau, Haro 6-10, HL Tau and HV Tau C. We do not find appreciable spatially extended  $\text{Br}\gamma$  in CW Tau, T Tau, XZ Tau, or RW Aur.

Figures 1 through 4 show the images of the spatially extended  $\text{Br}\gamma$  emission from DG Tau (Figure 1), Haro 6-10 (Figure 2), HL Tau (Figure 3) and HV Tau C (Figure 4). The panels in these figures show: a) - the continuum emission with contours of  $[\text{Fe II}]$  emission overplotted to demonstrate the outflow position and geometry, b) - continuum subtracted  $\text{Br}\gamma$  line emission maps with contours of the continuum overplotted, c) - “point-source subtracted” spatially extended maps of  $\text{Br}\gamma$  emission with the contours of the continuum-subtracted  $\text{Br}\gamma$  overplotted, and d) - images of the integrated blue-shifted  $\text{Br}\gamma$  emission only, with contours of the point-source subtracted  $\text{Br}\gamma$  emission overplotted. At the right side of each image is the key correlating the image intensity to flux. The continuum images in panels (a) were constructed by fitting a straight line to the continuum around the  $\text{Br}\gamma$  emission feature and integrating the linear fit through the velocity channels that correspond to the  $\text{Br}\gamma$  emission. The images of the total  $\text{Br}\gamma$  emission presented in the b) panels were constructed by subtracting the linear fit to the continuum from the datacubes, then integrating in velocity over the  $\text{Br}\gamma$  emission feature. The “point-source subtracted”  $\text{Br}\gamma$  images shown in the c) panels were derived by normalizing the continuum (PSF) image to the peak flux in each velocity channel through the  $\text{Br}\gamma$  emission datacube, subtracting this scaled continuum image off of the  $\text{Br}\gamma$  cube, and integrating over the velocity extent to form an image of only the extended emission. The image of spatially extended blue-shifted  $\text{Br}\gamma$  emission shown in panel d) was made by integrating the ‘point-source subtracted’ image in 2-3 velocity channels of blue-shifted emission only. The d) panels show that the spatially extended  $\text{Br}\gamma$  emission is stronger in the blue-shifted velocity channels. Because of Poisson statistics associated with the subtraction process, detection of spatially extended  $\text{Br}\gamma$  emission is less robust at distances of  $<0.1$  from the central point-source. The  $\text{Br}\gamma$  emission in the vicinity of HV Tau C is quite weak, and all of the detected line emission is spatially extended. As a result, Figure 4 presents only the (a) and (b) panels for HV Tau C.

For DG Tau and Haro 6-10 S, the majority of the  $\text{Br}\gamma$  emission that we detect, integrated over wavelength, is consistent with the stellar point-source image. For HL Tau and HV Tau C, the majority of the  $\text{Br}\gamma$  is not coincident with the central TTS. The integrated  $\text{Br}\gamma$  emission from DG Tau follows the point-source continuum contours with little deviation (Figure 1b). The spatially extended  $\text{Br}\gamma$  emission from DG Tau is detected in panel 1(c),

and seen clearly in the blue-shifted emission shown in panel 1(d). The Blue-shifted emission (Figure 1d) extends to the south-west of DG Tau, at an orientation and velocity consistent with the known, collimated blue-shifted jet. Haro 6-10 also shows the bulk of the Br $\gamma$  emission arising from the two stellar point-sources. However, strong emission comes from the same location as the [Fe II] outflow emission from Haro 6-10 S (Figure 2c). In fact, for Haro 6-10 S, the Br $\gamma$  arising from the outflow is  $\sim 20\%$  of the total spatially integrated Br $\gamma$  emission in some blue-shifted velocity channels (Figure 2d). No spatially extended Br $\gamma$  is detected toward the Haro 6-10 N component.

Data on HL Tau were acquired with the 0."2 occulting disk blocking the central stellar point-source, however an appreciable amount of the detected Br $\gamma$  emission is seen to deviate from the central stellar position. HL Tau shows strong spatially extended Br $\gamma$  that follows the scattered light nebulosity revealed in the continuum emission (Figure 3b, 3c; Takami et al. 2007; Close et al. 1997). The integrated blue-shifted Br $\gamma$  from HL Tau (Figure 2d) shows very weak emission detected at a  $4\sigma$  level of significance that corresponds precisely with the spatial location of the [Fe II] emission. HV Tau C is a system with a known circumstellar disk viewed nearly edge-on (Stapelfeldt et al. 2003) and the stellar continuum flux is much fainter than the other sources. Curiously, we find no significant Br $\gamma$  emission associated with the locations of the continuum flux. The Br $\gamma$  emission from HV Tau C is quite weak. It is spatially extended from the continuum and it appears to only follow the location of the outflow seen in [Fe II] (Figure 4).

The spatially extended Br $\gamma$  emission revealed in Figures 1, 2, and 4 for DG Tau, Haro 6-10 S, and HV Tau C, lies precisely along the outflow axis of the known Herbig-Haro energy flows associated with these young stars. For HL Tau, the detected (low signal-to-noise) Br $\gamma$  emission in the blue-shifted component of the emission (Figure 3d) arises from the same spatial location as the known blue-shifted outflow (Takami et al. 2007). However in HL Tau the majority of the spatially extended Br $\gamma$  emission (Figure 3c) is not appreciably shifted in velocity from the nominal stellar radial velocity; it is detected at much higher S/N, and appears to arise from Br $\gamma$  emission from the central point-source that has been scattered off of the wall of the outflow cavity (Close et al. 1997; Takami et al. 2007).

Figure 5 shows the velocity profiles of the Br $\gamma$  flux associated with the central point source for DG Tau, Haro 6-10, HL Tau and HV Tau C at the location of the peak continuum emission (upper panel) and the profiles of Br $\gamma$  emission extracted in 0."2 diameter apertures at "Position B" and "Position C" as designated in Figures 1 through 4 for each star. The spatially extended Br $\gamma$  from DG Tau and Haro 6-10 S is blue-shifted in velocity by  $> 100 \text{ km s}^{-1}$  with respect to the central point-source flux. HL Tau shows strong emission at the velocity of the point-source flux in "Position B," and very slight  $\sim 3\text{-}4\sigma$  detection of



flux from blue-shifted ( $\sim 200 \text{ km s}^{-1}$ ) emission from the outflow.

In DG Tau, Haro 6-10 S and HL Tau, the spatially extended Br $\gamma$  emission that we detect from the outflows corresponds to the blue-shifted regions of the jets. This is consistent with the fact that blue-shifted jet components are flowing into our line of sight, and are hence less obscured by intervening circumstellar disk material. HV Tau C is the only source where both blue and red-shifted Br $\gamma$  is detected from opposite sides of the outflow with respect to the (estimated) position of the central star. The extended Br $\gamma$  from HV Tau C is quite weak in some regions, it is detected at a low signal-to-noise but follows the location of the extended outflow. Curiously, we find that the blue-shifted outflow lies to the northeast, and the red-shifted emission is to the southwest, which (as predicted by Stapelfeldt et al. 2003) is at odds with the relative brightnesses of the lobes of the scattered light edge-on disk reflection nebula associated with this source. The southwestern lobe of the HV Tau C scattered light nebula is brighter, and was thus thought to be associated with the blue-shifted (closer) lobe of the outflow. Our data reveal that this is not the case, and the north-eastern, fainter lobe seems to be associated with more blue-shifted outflow emission.

Figure 6 presents the standard deviation of continuum subtracted Br $\gamma$  flux with increasing distance from the central star (plotted as a solid line) for HL Tau (a), DG Tau (b), Haro 6-10 (c) and HV Tau C (d). These curves were derived for each source by calculating the mean flux within  $0.''08$  wide pixel annuli from the central stellar position and computing the standard deviation from the mean. This standard deviation of continuum subtracted line emission provides a measure of the uncertainty in the subtraction process, and thus can be used to gauge the S/N of the spatially extended line emission. Though, the continuum subtracted plots do have the extended Br $\gamma$  flux included within the field. As a result, the measured standard deviations in the spatial bins with appreciable Br $\gamma$  flux are correspondingly higher, and the accuracy of the subtraction process is thus under-estimated. Overplotted in each of the four panels is a dashed line that shows the magnitude of the point-source subtracted Br $\gamma$  flux with increasing distance from the central stellar position. Comparison of the dashed curve with the solid curve provides an estimate of the measured S/N of the extended Br $\gamma$  emission. The peak S/N for extended Br $\gamma$  is  $\sim 7$  for HL Tau,  $\sim 5$  for DG Tau,  $\sim 25$  for Haro 6-10 S and  $\sim 4$  for HV Tau C.

Figure 7 plots the same standard deviation of continuum subtracted Br $\gamma$  flux with increasing distance from CW Tau, T Tau, XZ Tau, and RW Aur, and a dashed line is also over-plotted that presents the peak magnitude of the point-source subtracted Br $\gamma$  emission from the central star (in the case of the multiple systems, the central star is assumed to be the brightest stellar component). The stellar companion position locations are apparent in the plots for XZ Tau and T Tau, while RW Aur’s companion has a slightly greater separation



than presented in Figure 7d. For all four sources presented in Figure 7, no excess was seen in spatially extended Br $\gamma$  emission at the location of the known Herbig-Haro outflows. For the cases of CW Tau, XZ Tau and RW Aur, no strong evidence of extended Br $\gamma$  emission beyond a S/N of  $\sim 3$  is found. Curiously, XZ Tau B showed weak Br $\gamma$  emission associated with the position of the star, but XZ Tau A had no detectable Br $\gamma$ . This result is seemingly at odds with the proposition that XZ Tau A is the more actively accreting star and the main driving source of the Herbig-Haro flow associated with this system (Krist et al. 2008). Although RW Aur exhibits very strong, centralized Br $\gamma$  emission flux, RW Aur B showed no measurable Br $\gamma$  emission associated with stellar mass accretion from its circumstellar disk.

The central region of Br $\gamma$  emission for T Tau N was saturated in the data, making a proper measurement of the continuum subtracted Br $\gamma$  flux and point-source subtracted flux difficult. The surrounding spatial and spectral regions nearby are not saturated, and were used to estimate the 2.16  $\mu\text{m}$  flux level based on the shape of the PSF. A cursory fitting analysis done at velocities on and off of the emission line using the A 0 spectral type telluric calibrator as a PSF reference showed that the Br $\gamma$  emission associated with T Tau N is not appreciably extended compared to the point-source continuum emission. The line emission is asymmetric around the T Tau S PSF, and is brighter to the northwest at the location of T Tau Sb. Hence, the Br $\gamma$  line emission associated with the nearby 0."1 T Tau S a+b binary seems to arise preferentially from the *b* component, and it is stronger than the continuum flux (i.e., the T Tau Sb / Sa flux ratio is greater in Br $\gamma$ ). This causes the apparent enhancement in Br $\gamma$  emission at the position of the companion in Figure 7b. Extraction of the individual spectra of the blended components was not done because of the saturation of T Tau N, which would need to serve as a PSF calibrator.

#### 4. Br $\gamma$ Estimates of YSO Mass Accretion and Mass Outflow Rates

Muzerolle et al. (1998b) showed that the Br $\gamma$  line luminosity from young stars correlates with the mass accretion rate, as determined from UV excess emission. Hence, we now use our detected Br $\gamma$  line fluxes to derive mass accretion rate for the observed targets. Table 2 presents the total Br $\gamma$  emission line fluxes (i.e., integrated over all velocity channels) for each of the young stars in this study. The relation from Muzerolle et al. (1998b) assumed all detected Br $\gamma$  emission was associated with the stellar point-sources, so the line fluxes that we have included in Table 2 are the total integrated flux values, including emission detected in the outflowing gas. Also included in Table 2 are the adopted stellar parameters used to derive the mass accretion rates: the stellar mass, temperature, luminosity and visual extinction (Kenyon & Hartmann 1995; White & Ghez 2001; Hartigan & Kenyon 2003;

Doppmann et al. 2008). The stellar parameters seem consistent with our K-band spectra, so we do not rederive them from our data.

XZ Tau B, T Tau S and Haro 6-10 N are “infrared luminous companions” (IRCs) to their respective primaries, and the stellar parameters for these sources are much less certain (Koresko et al. 1997; White & Ghez 2001). The accretion activity and line of sight visual extinction toward the IRCs could also be variable (Ghez et al. 1991; Beck et al. 2001; Leinert et al. 2001; Beck et al. 2004). Moreover, T Tau S is itself a binary, and the bulk of the Br $\gamma$  emission that we detect arises not from the IRC but from the  $\sim$ M-type T Tau Sb companion (Duchêne et al. 2005). Haro 6-10 N was found by Doppmann et al. (2008) to have weak evidence of photospheric Na absorption features at 2.20  $\mu$ m, with a late spectral type and an infrared veiling value estimated to be in the range of 12-15. Similarly, XZ Tau B also has strong infrared veiling and a poorly determined spectral type. As a result, we do not try to estimate mass accretion rates for T Tau S, Haro 6-10 N or XZ Tau B. Column 7 of Table 2 presents the mass accretion rates ( $\dot{M}_{acc}$ ) derived for all of the other stars, using the relation from Muzerolle et al. (1998b) for the Br $\gamma$  line luminosity to accretion luminosity and the Virial Theorem treatment put forth by Gullbring et al. (1998).

The mass accretion rates derived for the eight stars in this study that have well determined stellar parameters lie in the range from less than  $4 \times 10^{-10} M_{\odot}$  for RW Aur B, to  $1.5 \times 10^{-7} M_{\odot}$  for T Tau N, with most sources in the range of  $10^{-8}$  to  $10^{-7} M_{\odot}$ . These values compare lie within the overall range of mass accretion rates derived for cTTSs (Muzerolle et al. 1998b; Gullbring et al. 1998). For the most part, the mass accretion rates that we derive here are similar to  $\dot{M}_{acc}$  values for these stars that have been derived from previous studies, within the associated uncertainties (e.g., Hartigan et al. 1995; Muzerolle et al. 1998; White et al. 2004). However, direct comparisons between mass accretion values for DG Tau, particularly, show a large discrepancy in our study. DG Tau has in the past exhibited a mass accretion value on the high side of the range for TTSS; around or just under  $10^{-6} M_{\odot} \text{ yr}^{-1}$ . Our derived mass accretion rate is an order of magnitude less than many previously published estimates (Hartigan et al. 1995; Muzerolle et al. 1998b). DG Tau is known to vary in flux and spectral characteristics on short time scales (Biscaya et al. 1997; Hessman & Guenther 1997; Bary et al. 2008). Bary et al. (2008) found a nightly average Br $\gamma$  equivalent width of 6.4 Å for seven nights of observations with a standard deviation of 20%. Therefore, the discrepancy we see in mass accretion rate toward DG Tau might be a result of both intrinsic stellar and accretion variability.

Also presented in column 8 of Table 2 is the Br $\gamma$  flux from the spatially extended outflows from DG Tau and Haro 6-10 S. For our analysis of Br $\gamma$  emission seen in the outflows, we extracted a region of Br $\gamma$  flux from the spatially extended jets from DG Tau and Haro 6-

10 (Figures 1d and 2d). Multi-epoch observations have shown that the average transverse proper motion of an outflow is  $\sim 0.''2$  to  $0.''3$  per year, or 28-42 AU at the  $\sim 140$  pc distance of Taurus (Torres et al. 2009). Both the DG Tau and Haro 6-10 S outflows are viewed at  $60-70^\circ$  inclination angles (Movsessian & Magakian 1999; Pyo et al. 2003), and the 28-42 AU extent in the outflow is also roughly consistent with the corresponding annual motion of an average flow velocity of  $\sim 200 \text{ km s}^{-1}$ ; e.g., material in the flow would move 28-42 AU/yr at the estimated geometry and velocity. For this reason, to capture the emitting flux from approximately one year of jet motion, we have extracted a segment,  $0.''3$  in extent, of the spatially resolved Br $\gamma$  emission along the jet axes for the DG Tau and Haro 6-10 S outflows. The width of the extraction box corresponds to a  $0.''2$  radius encircling the jet. The Br $\gamma$  emitting volume,  $V_{\text{HI}}$ , roughly corresponds to this area surrounding the jet, and is approximated by a cylinder of 28 AU ( $0.''2$ ) radius and 42 AU ( $0.''3$ ) height. The “one year” integrated Br $\gamma$  outflow emission fluxes for DG Tau and Haro 6-10 S extracted from these apertures are  $6.8 \times 10^{-16}$  and  $8.5 \times 10^{-16} \text{ erg s}^{-1} \text{ cm}^{-2}$ , respectively.

Under the assumption that the spatially extended Br $\gamma$  emission seen from DG Tau and Haro 6-10 S arises from thermally excited emission from optically-thin, post-shock regions of the outflows and behave as a Case B recombining gas (Baker & Menzel 1938; Brocklehurst 1971; Hummer & Storey 1987; Storey & Hummer 1995), we use a simple analysis to measure the mass outflow rate from these stars. Using the H I emission coefficients from Osterbrock (1989), the expression for the detected Br $\gamma$  flux can be described as:

$$F_{\text{Br}\gamma} = 1.2 \times 10^{-28} (N_e^2 V_{\text{HI}} / D^2) \quad (1)$$

where  $D$  is the distance to the emitting region in centimeters,  $N_e$  is the electron density, and  $V_{\text{HI}}$  is the volume of the emitting region (MKS units). The electron temperature is assumed to be  $\sim 10^4 \text{ K}$ , which is a reasonable estimate for the inner regions of YSO outflows. The mass of the emitting hydrogen in the spatially resolved regions of the outflow can be estimated as  $M_{\text{HI}} = m_p N_e V_{\text{HI}}$ . Merging this equation for the mass with the above equation for the flux gives:

$$M_{\text{HI}} = 1.5 \times 10^{-13} (F_{\text{Br}\gamma} V_{\text{HI}})^{1/2} D \quad (2)$$

We can thus solve for the mass of emitting hydrogen gas using the parameters of our measured Br $\gamma$  flux, the selected emission volume, and the assumed 140 pc distance to the stars, which is based on distances derived toward TTS within the Taurus star forming complex (Torres et al. 2009). For DG Tau, an H I mass of  $1.2 \times 10^{-8} M_\odot$  is derived, and for Haro 6-10 S this value is  $1.4 \times 10^{-8} M_\odot$ . The flux extraction volumes were chosen to be the same, so the difference

in the atomic hydrogen outflow masses between the two stars is determined by the difference in their detected Br $\gamma$  flux values. Having chosen the flux extraction volumes to correspond to the average *annual* proper motions of these jets, these estimates approximate the mass outflow rates for DG Tau and Haro 6-10 S in solar masses per year.

Based on this analysis, we derive average electron densities on the order of a few  $\times 10^4 \text{ cm}^{-3}$  for the DG Tau and Haro 6-10 S outflows. These densities are consistent with the large values of  $10^4$  to  $10^6 \text{ cm}^{-3}$  for  $N_e$  that are often found within the inner one hundred AU regions of young star outflows derived by inspecting [Fe II] and other forbidden emission species (Hartigan et al. 1995; Bacciotti & Eislöffel 1999; Hartigan & Morse 2007; Hartigan & Hillenbrand 2009). These electron densities are also very consistent with past values found in the inner DG Tau high velocity blue-shifted jet (Bacciotti & Eislöffel 1999; Coffey et al. 2008).

The hydrogen outflow rates of  $1.2 \times 10^{-8} M_{\odot} \text{ yr}^{-1}$  for DG Tau and  $1.4 \times 10^{-8} M_{\odot} \text{ yr}^{-1}$  for Haro 6-10 S represent lower limits for the true mass outflow levels derived in this manner. These mass outflow rates are underestimates of the true mass flow because only the fraction of the gas that has recently been heated by the shock radiates in the emission species that is studied. We also only detect the gas in the high velocity component of the outflow, not in lower velocity flow surrounding the jet axis (Bacciotti et al. 2000; Pyo et al. 2003). Moreover, the derived Br $\gamma$  flux in the outflowing volume was not corrected for any line of sight extinction effects which might further serve to increase the derived mass outflow rate, particularly in the obscured Class I star, Haro 6-10 S. Thus, we predict that the true  $\dot{M}_{out}$  values are greater than  $1.2 \times 10^{-8} M_{\odot} \text{ yr}^{-1}$  for DG Tau and more than  $1.4 \times 10^{-8} M_{\odot} \text{ yr}^{-1}$  for Haro 6-10 S.

## 5. Discussion

This study shows that not all H I Br $\gamma$  emission from classical TTS arises from magnetospheric accretion processes within a few radii from the central star. We detect spatially resolved Br $\gamma$  from DG Tau, Haro 6-10 S, HL Tau and HV Tau C, which represents 50% of the TTS systems in our sample. We do not spatially resolve Br $\gamma$  line emission in the environments of XZ Tau, RW Aur, T Tau and CW Tau. Two stars within these latter systems, RW Aur B and XZ Tau A, exhibit no Br $\gamma$  emission at all.

In two of the blue-shifted velocity channels, the spatially extended Br $\gamma$  from Haro 6-10 S makes up  $\sim 20\%$  of the total spatially integrated line flux. Integrated over the whole velocity width, about  $10 \pm 2\%$  of the Br $\gamma$  emission from Haro 6-10 S is spatially resolved at distances

of greater than  $0.''1$  (14 AU) in the extended outflow (entirely from the blue-shifted velocity component). The spatially extended Br $\gamma$  emission makes up  $\sim 2\%$  of the total line flux for DG Tau. All of the detected Br $\gamma$  flux seems to arise from the outflow for HV Tau C, but the star is not seen directly because the continuum flux is measured only from the scattered light nebulosity. The inner magnetospheric accretion region of HV Tau C may be shielded by the inner rim of the central circumstellar dust disk in our edge-on viewing orientation, hence in this case we might not see the strong central Br $\gamma$  component in the scattered light nebulosity. HL Tau has considerable Br $\gamma$  emission scattered off of its surrounding outflow cavity walls, and the fraction of spatially extended Br $\gamma$  emission is estimated to be  $18 \pm 7\%$  of the line flux from the central position. Observations of HL Tau were acquired with an occulting disk in the beam, so the total point source flux is estimated from the PSF shape in the target acquisition setup images and the resulting value is significantly less certain.

The majority of the integrated Br $\gamma$  flux that we measure is spatially unresolved from the position of the central stellar sources in our data, with the noted exception of the edge-on disk system HV Tau C. NIFS data can spatially resolve the bright Br $\gamma$  emission beyond  $\sim 0.''1$  from the star, or about  $\sim 14$  AU. Additional Br $\gamma$  emission likely arises from the outflows in regions closer than our resolution limit, where it cannot be detected. Overall, the extended Br $\gamma$  line emission that we detect beyond  $\sim 14$  AU distances from the parent stars comprises anywhere from a few percent (DG Tau) to all of the detected line flux from these systems (HV Tau C).

All of the sources that we have studied here are known to drive Herbig-Haro outflows. It is not clear why some stars exhibit extended Br $\gamma$  emission, while other sources with strong and collimated outflows do not. However, from information presented in Table 2, we see that the stars that have appreciable spatially extended Br $\gamma$  emission also have stronger estimated levels of optical visual extinction,  $A_v$ , toward the stellar photosphere. The stars where we do not find extended Br $\gamma$  emission all have lower estimated optical obscurations. In the systems where extended Br $\gamma$  emission is seen, the stronger levels of stellar continuum flux attenuation from the high visual extinction may make the weak spatially extended emission easier to detect. The stars that do not exhibit extended Br  $\gamma$  emission have brighter stellar continuum flux, which may be a result of less obscuration by natal material because of a slightly older evolutionary state, or a perhaps a more inclined viewing geometry that directly reveals more of the central photosphere of the star. Thus, spatially extended Br $\gamma$  emission may exist toward the other stars, but the bright continuum flux might prevent us from detecting it.

Several recent spectro-astrometric and interferometric investigations of inner YSO disks have sought to spatially resolve the atomic hydrogen associated with the magnetospheric

recombination regions within 1 AU from the target stars (Whelan et al. 2004; Eisner et al. 2009; Kraus et al. 2008). The spectro-astrometric study of Whelan et al. (2004) revealed that an appreciable amount of  $\text{Pa}\beta$  emission from the blue and red-shifted velocity profiles arises from spatially extended distances from a TTS. Three of their four targets exhibited spatially resolved  $\text{Pa}\beta$  emission, two revealed evidence for spatially extended bi-polar red and blue-shifted components. This is an important finding, since the broadened emission line wings seen in the H I profiles from cTTS have never been well explained by magnetospheric accretion models. Evidence from this  $\text{Pa}\beta$  study and now our  $\text{Br}\gamma$  project suggest that the H I emission from TTS does have non-negligible components from the outflow on spatial scales that were unresolvable prior to the current generation of sensitive instrumentation on 8-10 meter class telescopes.

Thus far, spectro-interferometric studies of  $\text{Br}\gamma$  that can spatially resolve the inner magnetospheric accretion region have largely concentrated on the brighter Herbig Ae/Be stars (HAEBEs; Eisner et al. (2009); Kraus et al. (2008); Malbet et al. (2007)). Interestingly, most interferometric data reveals that the  $\text{Br}\gamma$  emission surrounding the HAEBEs arises from a centralized location that is spatially more compact than the infrared continuum emission, with perhaps some contribution from an outflowing wind (Malbet et al. 2007). The compact H I likely arises predominantly from the accretion-driven processes within the star-disk boundary; either from the central stellar mass accretion engine or from a stellar or disk wind (Kraus et al. 2008; Malbet et al. 2007; Eisner et al. 2010). Further work is warranted to better reveal the central emission location of H I from TTSs, and the fraction of H I emission that is truly spatially extended from the parent star in comparison to the higher mass HAEBEs.

Although we do detect spatially extended  $\text{Br}\gamma$  emission from 50% of our sample targets, the bulk of the line emission from most stars does arise within  $\sim 14$  AU from the central unresolved point sources. While the spatially extended H I seems to affect the wings of the velocity line profile shapes (Whelan et al. 2004), it is likely that the majority of the low velocity H I is emitted via magnetospheric processes in the central disk-star accretion region. Bary et al. (2008) presented a large-scale multi-epoch near-infrared spectroscopic survey of 15 actively accreting TTS in Taurus-Auriga. They compared the H I line ratios of 16 Paschen and Brackett series emission features and found little variations in these ratios from epoch to epoch and from source to source. For the first time, a statistically significant correlation was found between the observed H I line ratios in TTS systems and those predicted by Case B line recombination theory (Baker & Menzel 1938; Hummer & Storey 1987; Storey & Hummer 1995) for a tightly constrained gas temperature and electron density. While the range of electron densities Bary et al. find for the emitting H I gas agrees with that predicted by magnetospheric accretion models, the temperatures are substantially



lower than expected for accreting gas<sup>2</sup>. These results suggest that the emission is from a recombining gas not in local thermodynamic equilibrium and is instead being stimulated by a non-thermal process. In addition, these results may also suggest a combination of emission sources for the emitting H I gas in the central regions and that the observed H I line fluxes are a superposition of emitting gas with different physical conditions. As such, one might not necessarily expect a linear correlation between detected Br $\gamma$  flux from the central star and the liberated accretion luminosity measured from the UV excess emission, as found by Muzerolle et al. (1998b). However, the correlation does exist and the mass accretion rates we derived from our measured Br $\gamma$  line fluxes are consistent with those found in past studies of TTS. Taken in combination, these results further confirm the connection between accretion and outflow activity.

Deriving accurate mass outflow values is notoriously difficult. This is in part because the emission line regions in outflows measure only material in the post-shock area of a jet and do not sample outflow material ahead of the shock. Shocks from outflows and their associated optical and infrared emission lines are obvious observational manifestations of mass outflow activity, but they are the result of fast material plowing into slower clumps of gas in the outflow path. Hence, material can (and does) exist in the outflow without these detectable emission features if there is no slower material in the flow path to cause the shock. Methods described in the literature for measuring mass outflow rates from classical TTSs rely largely on measuring the mass flux from forbidden emission line species and converting this to an outflow rate based on estimates of the gas ionization fraction (Hartigan et al. 1995; Cabrit 2002; Dougados et al. 2002; Bacciotti et al. 2002; Coffey et al. 2008; Agra-Amboage et al. 2009). The different observational techniques derive mass outflow to mass accretion ratios in the range of 1 to 10%. In some cases, multi-wavelength or emission line studies of the same system find  $\dot{M}_{out}/\dot{M}_{acc}$  values that differ by factors of  $\sim 10$ , even for the same system (e.g., DG Tau, see below). Measurement of mass outflow rates using atomic hydrogen emission species has been difficult in the past because of the strong optical depth effects in optical Balmer emission species. The infrared Brackett features are less optically thick, and may serve as a more robust tracer of the atomic hydrogen gas mass in the young star outflows.

In the previous section, we derived the first masses of ionized hydrogen using Br $\gamma$  emission for the DG Tau and Haro 6-10 S outflows. Comparison of the mass accretion rates with our derived atomic hydrogen mass outflow rates for DG Tau and Haro 6-10 S (see Table 2) reveals that the outflowing H I mass is estimated at  $\sim 10$ -15% of the mass accreting onto the central star. Moreover, our derived mass outflow rates are also lower limits,

---

<sup>2</sup>Bary et al. (2008) found the most likely temperature and density ranges of  $T < 2000$  K and  $10^9 \text{ cm}^{-3} < n_e \leq 10^{10} \text{ cm}^{-3}$ .



implying that the actual ratio of  $\dot{M}_{out}/\dot{M}_{acc}$  may be larger than 10-15% for these two sources. These ratios are consistent with  $\dot{M}_{out}/\dot{M}_{acc}$  values predicted by the theory of mass accretion efficiency and magnetocentrifugal launching mechanisms (i.e., disk winds and accretion-driven stellar winds) for young star outflows (Koenigl 1991; Matt & Pudritz 2005; Cranmer 2008), and are on the high side in comparison with ratios found from other observational investigations (Edwards et al. 1987; Hartigan et al. 1995; Cabrit 2002; Dougados et al. 2002; Bacciotti & Eisloffel 1999; Coffey et al. 2008; Agra-Amboage et al. 2009).

It is interesting that we find  $\dot{M}_{out}/\dot{M}_{acc}$  values for DG Tau and Haro 6-10 S that seem in the high range compared to ratios derived from other observations. Additionally, the  $\dot{M}_{out}$  rates we find are lower limits, as discussed in §5. However, the uncertainties in the derivation of both the  $\dot{M}_{out}$  and  $\dot{M}_{acc}$  values can be very large. Our lower limit for the value of  $\dot{M}_{out}$  in DG Tau and Haro 6-10 S is derived from straightforward assumptions on the physics of LTE atomic hydrogen in recombination regions. As noted above, the hydrogen recombination emission area very close to the central star is possibly excited by non-thermal processes in the inner magnetospheric region (Bary et al. 2008). Hence, it seems feasible that these non-LTE conditions may extend into the inner regions of the outflow, making our H II-like analysis of hydrogen emitting mass correspondingly uncertain. This is likely one of the largest sources of uncertainty in our analysis, but it is also difficult to characterize. We also estimate an additional source of error in our selection of the emission volume that was chosen to represent one year worth of jet motion. Moreover, the correlation of integrated Br $\gamma$  line luminosity with stellar mass accretion luminosity has an intrinsic scatter (Muzerolle et al. 1998b), and deviation in  $\dot{M}_{out}/\dot{M}_{acc}$  by a factor of several for a given target can result from using this method to derive the stellar mass accretion rate. Multiple observations of accretion indicators from large sample of TTS demonstrate the highly variable nature of accretion activity in these young stars (e.g., Bary et al. 2008; Nguyen et al. 2009). However, the effects from intrinsic time variation in the accretion and outflow properties are not an issue in our study because the mass outflow and mass accretion rates are derived simultaneously from the same data set.

The blue-shifted jet emerging from DG Tau is arguably one of the best studied outflows associated with a young star. It was among the first cTTSs for which a collimated jet-like outflow was discovered (Mundt & Fried 1983). Since its discovery, the HH 158 outflow from DG Tau has been investigated with high spatial resolution imaging and spectroscopy with *HST*, ground-based adaptive optics systems, and spectro-imaging techniques (Lavalley et al. 1997; Lavalley-Fouquet et al. 2000; Bacciotti et al. 2000; Dougados et al. 2002; Bacciotti et al. 2003; Pyo et al. 2003; Takami et al. 2004; Coffey et al. 2008). This outflow has observationally revealed the structure of collimated YSO jets in great spatial detail; they are typically comprised of an on-axis high velocity component (HVC) at radial velocities greater than

$\sim 50 \text{ km s}^{-1}$  that can extend to spatial distances of hundreds of AU from the star, and an encompassing shell of lower velocity gas that extends only about  $\sim 100$  AU away from the central star (Bacciotti et al. 2000; Pyo et al. 2003; Takami et al. 2004). Although He I 10830 emission is commonly attributed only to stellar winds in the inner  $\sim 10$  AU environments of CTTS, Takami et al. (2002) detect He I 10830 emission from DG Tau at the jet velocity, spatially extended over  $\sim 0.5$  arcsec ( $\sim 70$  AU) of the jet, though their spectroastrometry did not find extension in the low-velocity He I 10830 emission. Bacciotti et al. (2000) and Pyo et al. (2003) described the blue-shifted HH 158 jet as having an “onion-skin” structure, with high velocity low density gas on-axis, surrounded by successive layers of lower velocity, higher density gas. Integrated over the width of the jet axis, the  $\dot{M}_{out}/\dot{M}_{acc}$  values derived for the DG Tau jet from past studies lie in the range of 0.05-0.1 (Lavalley et al. 1997; Bacciotti et al. 2000; Coffey et al. 2008), though most of these estimates use large mass accretion rate of  $\sim 10^6 \text{ M}_{\odot} \text{ yr}^{-1}$  (Hartigan et al. 1995). Bacciotti et al. (2003) analyzed the kinematics of DG Tau’s jet and found evidence for velocity asymmetries across the jet axis, and they interpret this result as evidence for rotation within the inner jet channel. This controversial finding challenges the theories of magnetospheric interaction at the inner star + disk + outflow boundary region.

The outflow from DG Tau has served as a laboratory to test the physics of YSO jets, so it is fitting that our first discovery of spatially extended Br $\gamma$  from cTTSS includes this system. In DG Tau, the spatially extended Br $\gamma$  emission that we detect arises from the high velocity, on-axis gas in the blue-shifted outflow. Interestingly, this H I coincides very closely in projected location with the recently discovered X-ray emission in the jet (Güdel et al. 2005, 2008). Güdel et al. (2008) found that the blue-shifted outflow from DG Tau has emission from soft X-rays out to spatially extended distances of several hundred AU from the central star. The temperatures of the soft X-ray emission regions associated with the extended X-ray jet are on the order of a few times  $10^6 \text{ K}$ . These temperatures pose a problem for understanding jet heating mechanisms. The standard jet shock models for YSO outflows cannot explain temperatures on the order of  $10^6 \text{ K}$ , and this argues strongly in favor of some form of non-thermal excitation of the gas; for example by Ohmic heating from magnetic dissipative currents (Güdel et al. 2008). The detected Br $\gamma$  emission from the DG Tau blue-shifted outflow seems to correspond to gas nearby to these super-heated regions, and thus if strong magnetic fields significantly effect the physical conditions in the inner flows then our simple method of deriving  $\dot{M}_{out}$  assuming thermal Case B recombination of atomic hydrogen at temperatures of  $\sim 10^4 \text{ K}$  would be correspondingly inaccurate. Further tests and comparison of the physical conditions in Br $\gamma$  and X-ray emitting jets could help clarify the physics in the inner regions of the outflows. Unfortunately, as previously mentioned, HL Tau, HV Tau C and Haro 6-10 S are Class I protostars or cTTSS with circumstellar disks viewed

in a nearly edge-on configuration, and all three of these systems have very strong optical obscuration (see Table 2). It is likely not feasible to detect the soft X-ray emission from these jets to further test the physical conditions of the Br $\gamma$  emission environments.

## 6. Summary

We have presented the results of our K-band integral field spectroscopy study of the Br $\gamma$  line emission from eight T Tauri star systems. The key points of our study are:

1) Using adaptive optics fed integral field spectroscopy, we have spatially resolved Br $\gamma$  line emission in the circumstellar environments around four of our eight survey target stars: DG Tau, Haro 6-10 S, HL Tau and HV Tau C.

2) The spatially extended Br $\gamma$  emission arises predominantly from the hydrogen recombination regions associated with the inner Herbig-Haro outflows from these young stars. Only HL Tau shows a significant contribution of stellar Br $\gamma$  emission scattered into our line of sight off of the outflow cavity walls. This emission from HL Tau has a similar morphology to the scattered light continuum flux, and it likely originated from the inner magnetospheric accretion region around the star.

3) At some blue-shifted velocities, the spatially extended Br $\gamma$  emission comprises  $\sim 20\%$  of the detected Br $\gamma$  (e.g., Haro 6-10). Although we spatially resolve Br $\gamma$  emission from outflows in our high-contrast measurements, the majority of the integrated Br $\gamma$  from most systems is spatially unresolved and may arise from the magnetospheric accretion processes at the location of the central stellar source (with the exception of HV Tau C).

4) All of the Br $\gamma$  emission that we detect above the continuum flux from HV Tau C is from the spatially extended emission, consistent with the location of the known Herbig-Haro outflow. HV Tau C is seen in continuum light as a scattered light edge-on disk nebula. The inner magnetospheric component of Br $\gamma$  flux may be shielded from our line of sight by material in the inner edge of the circumstellar disk.

5) Derivation of the stellar mass accretion rates from the relationship between Br $\gamma$  line luminosity and mass accretion reveal  $\dot{M}_{acc}$  values that are typical of cTTSs.

6) Detection of the spatially extended Br $\gamma$  emission from the outflows in the DG Tau and Haro 6-10 S systems have allowed us to derive a value for the emitting hydrogen mass outflow rate using simple arguments applicable to hydrogen recombination regions. The corresponding values for  $\dot{M}_{out}/\dot{M}_{acc}$  that we derive are on the order of  $\sim 10\text{--}15\%$ , consistent with many prediction from accretion-driven stellar winds and disk winds, while on the high

side in comparison to observationally derived mass outflow to accretion rate ratios from past studies.

7) We find that in some young protostars, Br $\gamma$  emission extended on spatial scales of greater than 0."1 (14 AU) can contribute  $\sim 10\%$  of the flux to the detected integrated line emission (or more, as in the case of HL Tau and HV Tau C).

Several NIFS datasets presented in this study were acquired during the early stages of instrument integration at Gemini North Observatory, and we are extremely grateful for the support of the NIFS teams at the Australian National University, Auspace, and Gemini Observatory for their tireless efforts during the instrument commissioning and system verification. This study is based on data from the Gemini Observatory, which is operated by the Association of Universities for Research in Astronomy, Inc., on behalf of the international Gemini partnership of Argentina, Australia, Brazil, Canada, Chile, the United Kingdom, and the United States of America.

## REFERENCES

- Agra-Amboage, V., Dougados, C., Cabrit, S., Garcia, P. J. V., & Ferruit, P. 2009, *A&A*, 493, 1029
- Bacciotti, F., & Eislöffel, J. 1999, *A&A*, 342, 717
- Bacciotti, F., Mundt, R., Ray, T. P., Eislöffel, J., Solf, J., & Camezind, M. 2000, *ApJ*, 537, L49
- Bacciotti, F., Ray, T. P., Eislöffel, J., Woitas, J., Solf, J., Mundt, R., & Davis, C. J. 2003, *Ap&SS*, 287, 3
- Bacciotti, F., Ray, T. P., Mundt, R., Eislöffel, J., & Solf, J. 2002, *ApJ*, 576, 222
- Bailey, J. 1998, *MNRAS*, 301, 161
- Baker, J. G., & Menzel, D. H. 1938, *ApJ*, 88, 52
- Bary, J. S., Matt, S. P., Skrutskie, M. F., Wilson, J. C., Peterson, D. E., & Nelson, M. J. 2008, *ApJ*, 687, 376
- Beck, T. L., McGregor, P. J., Takami, M., & Pyo, T. 2008, *ApJ*, 676, 472
- Beck, T. L., Prato, L., & Simon, M. 2001, *ApJ*, 551, 1031

- Beck, T. L., Schaefer, G. H., Simon, M., Prato, L., Stoesz, J. A., & Howell, R. R. 2004, *ApJ*, 614, 235
- Bertout, C., Basri, G., & Bouvier, J. 1988, *ApJ*, 330, 350
- Biscaya, A. M., Rieke, G. H., Narayanan, G., Luhman, K. L., & Young, E. T. 1997, *ApJ*, 491, 359
- Brannigan, E., Takami, M., Chrysostomou, A., & Bailey, J. 2006, *MNRAS*, 367, 315
- Brocklehurst, M. 1971, *MNRAS*, 153, 471
- Cabrit, S. 2002, in *EAS Publications Series*, Vol. 3, *EAS Publications Series*, ed. J. Bouvier & J.-P. Zahn, 147–182
- Close, L. M., Roddier, F., Northcott, M. J., Roddier, C., & Graves, J. E. 1997, *ApJ*, 478, 766
- Coffey, D., Bacciotti, F., & Podio, L. 2008, *ApJ*, 689, 1112
- Cranmer, S. R. 2008, *ApJ*, 689, 316
- Doppmann, G. W., Najita, J. R., & Carr, J. S. 2008, *ApJ*, 685, 298
- Dougados, C., Cabrit, S., & Lavalley-Fouquet, C. 2002, in *Revista Mexicana de Astronomia y Astrofisica Conference Series*, Vol. 13, *Revista Mexicana de Astronomia y Astrofisica Conference Series*, ed. W. J. Henney, W. Steffen, L. Binette, & A. Raga, 43–48
- Duchêne, G., Ghez, A. M., McCabe, C., & Ceccarelli, C. 2005, *ApJ*, 628, 832
- Edwards, S., Cabrit, S., Strom, S. E., Heyer, I., Strom, K. M., & Anderson, E. 1987, *ApJ*, 321, 473
- Eisenhauer, F., Tecza, M., Mengel, S., Thatte, N. A., Roehrle, C., Bickert, K., & Schreiber, J. 2000, in *Society of Photo-Optical Instrumentation Engineers (SPIE) Conference Series*, Vol. 4008, *Society of Photo-Optical Instrumentation Engineers (SPIE) Conference Series*, ed. M. Iye & A. F. Moorwood, 289–297
- Eisner, J. A., et al. 2010, *ApJ*, 718, 774
- Eisner, J. A., Graham, J. R., Akeson, R. L., & Najita, J. 2009, *ApJ*, 692, 309
- Garcia, P. J. V., Thiébaut, E., & Bacon, R. 1999, *A&A*, 346, 892

- Ghez, A. M., Neugebauer, G., Gorham, P. W., Haniff, C. A., Kulkarni, S. R., Matthews, K., Koresko, C., & Beckwith, S. 1991, *AJ*, 102, 2066
- Güdel, M., Skinner, S. L., Audard, M., Briggs, K. R., & Cabrit, S. 2008, *A&A*, 478, 797
- Güdel, M., Skinner, S. L., Briggs, K. R., Audard, M., Arzner, K., & Telleschi, A. 2005, *ApJ*, 626, L53
- Gullbring, E., Hartmann, L., Briceno, C., & Calvet, N. 1998, *ApJ*, 492, 323
- Hartigan, P., Edwards, S., & Ghandour, L. 1995, *ApJ*, 452, 736
- Hartigan, P., & Hillenbrand, L. 2009, *ApJ*, 705, 1388
- Hartigan, P., & Kenyon, S. J. 2003, *ApJ*, 583, 334
- Hartigan, P., & Morse, J. 2007, *ApJ*, 660, 426
- Hessman, F. V., & Guenther, E. W. 1997, *A&A*, 321, 497
- Hummer, D. G., & Storey, P. J. 1987, *MNRAS*, 224, 801
- Kenyon, S. J., & Hartmann, L. 1995, *ApJS*, 101, 117
- Koenigl, A. 1991, *ApJ*, 370, L39
- Koresko, C. D., Herbst, T. M., & Leinert, C. 1997, *ApJ*, 480, 741
- Kraus, S., Hofmann, K., Benisty, M., Berger, J., Chesneau, O., Isella, A., Malbet, F., Meilland, A., Nardetto, N., Natta, A., Preibisch, T., Schertl, D., Smith, M., Stee, P., Tatulli, E., Testi, L., & Weigelt, G. 2008, *A&A*, 489, 1157
- Krist, J. E., Stapelfeldt, K. R., Hester, J. J., Healy, K., Dwyer, S. J., & Gardner, C. L. 2008, *AJ*, 136, 1980
- Larkin, J., Barczys, M., Krabbe, A., Adkins, S., Aliado, T., Amico, P., Brims, G., Campbell, R., Canfield, J., Gasaway, T., Honey, A., Iserlohe, C., Johnson, C., Kress, E., Lafreniere, D., Magnone, K., Magnone, N., McElwain, M., Moon, J., Quirrenbach, A., Skulason, G., Song, I., Spencer, M., Weiss, J., & Wright, S. 2006, *New Astronomy Review*, 50, 362
- Lavalley, C., Cabrit, S., Dougados, C., Ferruit, P., & Bacon, R. 1997, *A&A*, 327, 671
- Lavalley-Fouquet, C., Cabrit, S., & Dougados, C. 2000, *A&A*, 356, L41

- Leinert, C., Beck, T. L., Ligorì, S., Simon, M., Woitas, J., & Howell, R. R. 2001, *A&A*, 369, 215
- Lynden-Bell, D., & Pringle, J. E. 1974, *MNRAS*, 168, 603
- Malbet, F., et al. 2010, arXiv:1007.5382
- Malbet, F., et al. 2007, *A&A*, 464, 43
- Matt, S., & Pudritz, R. E. 2005, *MNRAS*, 356, 167
- McGregor, P. J., Hart, J., Conroy, P. G., Pfitzner, M. L., Bloxham, G. J., Jones, D. J., Downing, M. D., Dawson, M., Young, P., Jarnyk, M., & Van Harmelen, J. 2003, in *Society of Photo-Optical Instrumentation Engineers (SPIE) Conference Series*, Vol. 4841, *Society of Photo-Optical Instrumentation Engineers (SPIE) Conference Series*, ed. M. Iye & A. F. M. Moorwood, 1581–1591
- Mohanty, S., Jayawardhana, R., & Barrado y Navascués, D. 2003, *ApJ*, 593, L109
- Mohanty, S., Jayawardhana, R., & Basri, G. 2005, *ApJ*, 626, 498
- Movsessian, T. A., & Magakian, T. Y. 1999, *A&A*, 347, 266
- Mundt, R., & Fried, J. W. 1983, *ApJ*, 274, L83
- Muzerolle, J., Calvet, N., & Hartmann, L. 1998a, *ApJ*, 492, 743
- Muzerolle, J., Hartmann, L., & Calvet, N. 1998b, *AJ*, 116, 2965
- Najita, J., Carr, J. S., & Tokunaga, A. T. 1996, *ApJ*, 456, 292
- Natta, A., Testi, L., Muzerolle, J., Randich, S., Comerón, F., & Persi, P. 2004, *A&A*, 424, 603
- Nguyen, D. C., Scholz, A., van Kerkwijk, M. H., Jayawardhana, R., & Brandeker, A. 2009, *ApJ*, 694, L153
- Osterbrock, D. E. 1989, *Astrophysics of gaseous nebulae and active galactic nuclei*, ed. Osterbrock, D. E.
- Pontoppidan, K. M., Blake, G. A., van Dishoeck, E. F., Smette, A., Ireland, M. J., & Brown, J. 2008, *ApJ*, 684, 1323



- Pyo, T., Kobayashi, N., Hayashi, M., Terada, H., Goto, M., Takami, H., Takato, N., Gaessler, W., Usuda, T., Yamashita, T., Tokunaga, A. T., Hayano, Y., Kamata, Y., Iye, M., & Minowa, Y. 2003, *ApJ*, 590, 340
- Stapelfeldt, K. R., Ménard, F., Watson, A. M., Krist, J. E., Dougados, C., Padgett, D. L., & Brandner, W. 2003, *ApJ*, 589, 410
- Storey, P. J., & Hummer, D. G. 1995, *MNRAS*, 272, 41
- Takami, M., Bailey, J., & Chrysostomou, A. 2003, *A&A*, 401, 655
- Takami, M., Bailey, J., Gledhill, T. M., Chrysostomou, A., & Hough, J. H. 2001, *MNRAS*, 323, 177
- Takami, M., Beck, T. L., Pyo, T., McGregor, P., & Davis, C. 2007, *ApJ*, 670, L33
- Takami, M., Chrysostomou, A., Bailey, J., Gledhill, T. M., Tamura, M., & Terada, H. 2002, *ApJ*, 568, L53
- Takami, M., Chrysostomou, A., Ray, T. P., Davis, C., Dent, W. R. F., Bailey, J., Tamura, M., & Terada, H. 2004, *A&A*, 416, 213
- Torres, R. M., Loinard, L., Mioduszewski, A. J., & Rodríguez, L. F. 2009, *ApJ*, 698, 242
- Uchida, Y., & Shibata, K. 1984, *PASJ*, 36, 105
- Whelan, E. T., Ray, T. P., & Davis, C. J. 2004, *A&A*, 417, 247
- White, R. J., & Ghez, A. M. 2001, *ApJ*, 556, 265

Table 1. Observing Log

Star Name	HH #	Obs. Date (UT)	PA of Obs.	Exp Time/Coads	# Exp	Total Exposure Time	Note on Obs.
T Tau	HH 255	2005 Oct 25	0°	5.3s/24	36	4580s	AO Flexure Test
RW Aur	HH 229	2005 Oct 22	221°	40s/1	11	440s	AO Guide Test
XZ Tau	HH 152	2005 Oct 25	0°	30s/1	28	820s	AO+OIWFS* Guide Test
DG Tau	HH 158	2005 Oct 26	0°	20s/6	101	12120s	AO+OIWFS* Flexure Test
HV Tau C	HH 233	2005 Oct 22	114°	900s/1	3	2700s	System Sensitivity Test
HL Tau	HH 150	2006 Feb 12	146°	900s/1	3	2700s	0.''2 Occulting Disk SV
CW Tau	HH 150	2006 Dec 5	146°	900s/1	3	2700s	NIFS PI GT
Haro 6-10	HH 150	2007 Feb 7 & 8	0°	300s/1	9	2700s	NIFS + LGS AO Queue

\*The NIFS On-Instrument WaveFront Sensor (OIWFS) is used to correct spatial flexure in the observations.

Table 2. Stellar Parameters and Mass Accretion Rates

Star	Mass $M_{\odot}$	Luminosity $L_{\odot}$	$T_{eff}$ K	$A_v$ mag	Integrated Br $\gamma$ Flux $W/m^2$	$\dot{M}_{acc}$ $M_{\odot} \text{ yr}^{-1}$	$\dot{M}_{out}$ $M_{\odot} \text{ yr}^{-1}$	Reference
(1)	(2)	(3)	(4)	(5)	(6)	(7)	(8)	(9)
CW Tau	1.1	0.7	4700	2.2	$1.5 \times 10^{-16}$	$1.3 \times 10^{-08}$	...	Doppmann et al.
DG Tau	2.2	7.7	4775	3.3	$4.5 \times 10^{-16}$	$9.6 \times 10^{-08}$	$> 1.2 \times 10^{-08}$	
Haro 6-10 S	0.7	1.8	4000	12.1	$7.2 \times 10^{-17}$	$6.7 \times 10^{-08}$	$> 1.4 \times 10^{-08}$	
HL Tau	1.2	3.0	4400	7.4	$2.1 \times 10^{-16}$	$8.7 \times 10^{-08}$	...	
RW Aur A	2.8	12.9	5000	1.6	$7.2 \times 10^{-16}$	$1.4 \times 10^{-07}$	...	
RW Aur B	1.2	3.0	4200	1.6	$< 5.1 \times 10^{-18}$	$< 4.1 \times 10^{-10}$	...	
T Tau N	2.1	7.2	5250	1.5	$8.4 \times 10^{-16}$	$1.5 \times 10^{-07}$	...	
XZ Tau A	0.45	0.4	3400	1.4	$< 7.7 \times 10^{-18}$	$< 1.9 \times 10^{-09}$	...	Doppmann et al.
XZ Tau B								
Haro 6-10 N	0.6	0.8	4100	29.0	$1.7 \times 10^{-17}$	$4.6 \times 10^{-08}$	...	

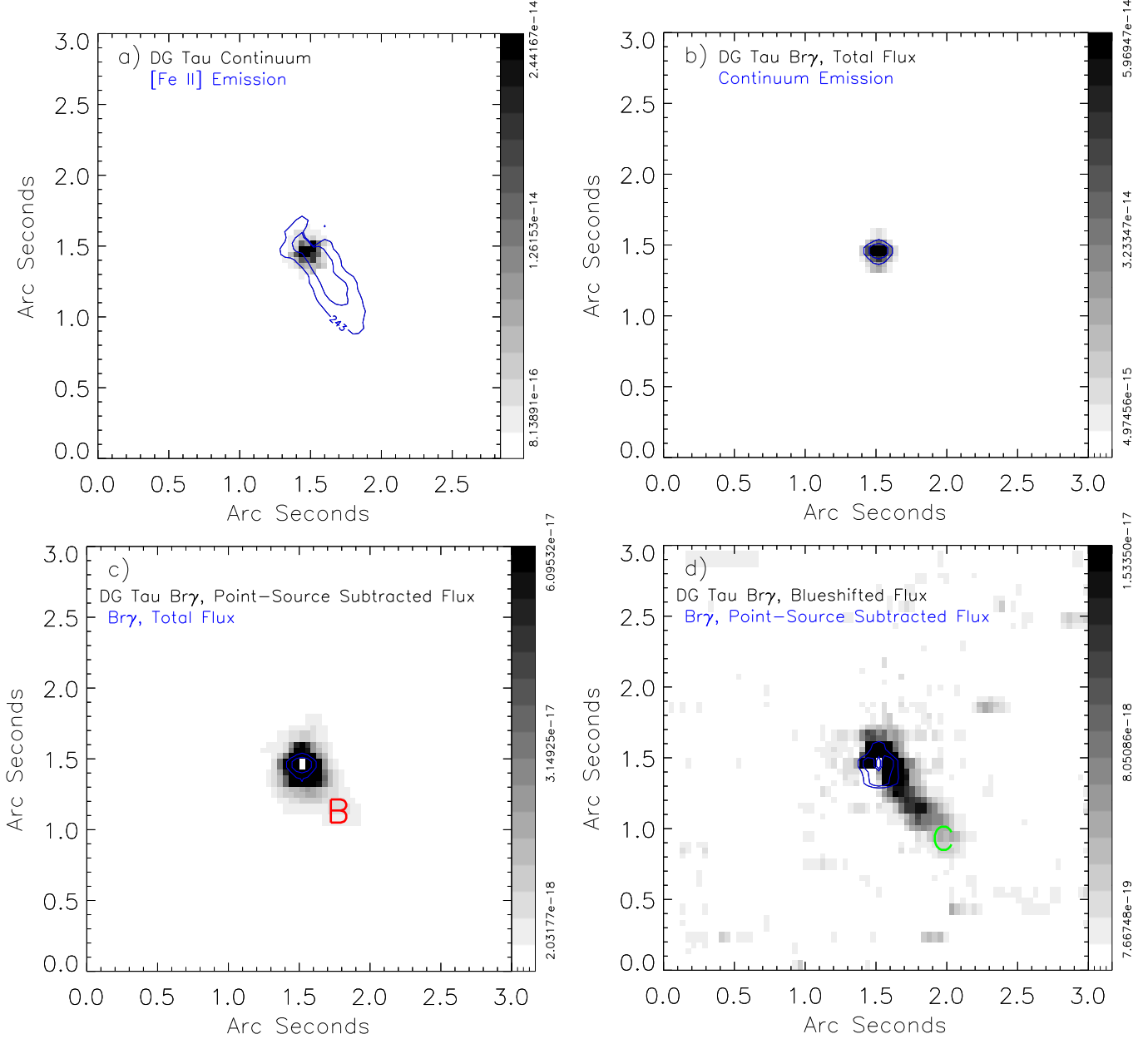


Fig. 1.— (a) The  $2.16\ \mu\text{m}$  continuum flux level from DG Tau with contours of [Fe II] emission overplotted, designating the outflow location, (b) the continuum subtracted point-source Br $\gamma$  flux and (c) the continuum and point-source subtracted map of spatially extended Br $\gamma$  from DG Tau. Also included here is a continuum and point-source subtracted map of spatially extended Br $\gamma$ , integrated over only three blue-shifted velocity channels (d). The (d) panels show that much of the spatially extended Br $\gamma$  emission is blue-shifted. The locations designated as "B" and "C" had 1-D spectral traces extracted, these are presented in Figure 5.

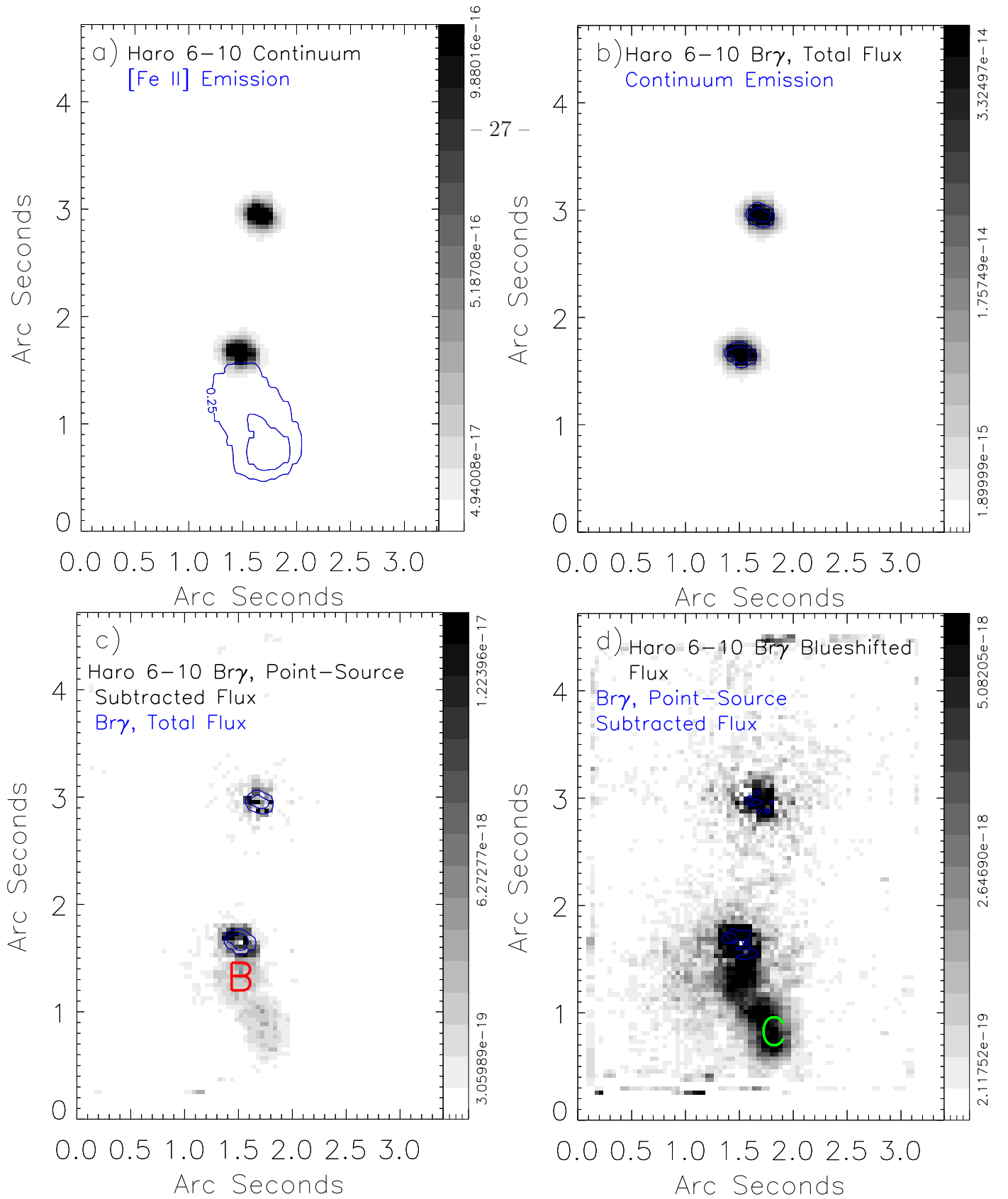


Fig. 2.— (a) The  $2.16\ \mu\text{m}$  continuum flux level from Haro 6-10 with contours of [Fe II] emission overplotted, designating the outflow location, (b) the continuum subtracted point-source Br $\gamma$  flux and (c) the continuum and point-source subtracted map of spatially extended Br $\gamma$  from Haro 6-10 S. Also included here is a continuum and point-source subtracted map of spatially extended Br $\gamma$ , integrated over only three blue-shifted velocity channels (d). The (d) panels show that much of the spatially extended Br $\gamma$  emission is blue-shifted. The locations designated as "B" and "C" had 1-D spectral traces extracted, these are presented in Figure 5.

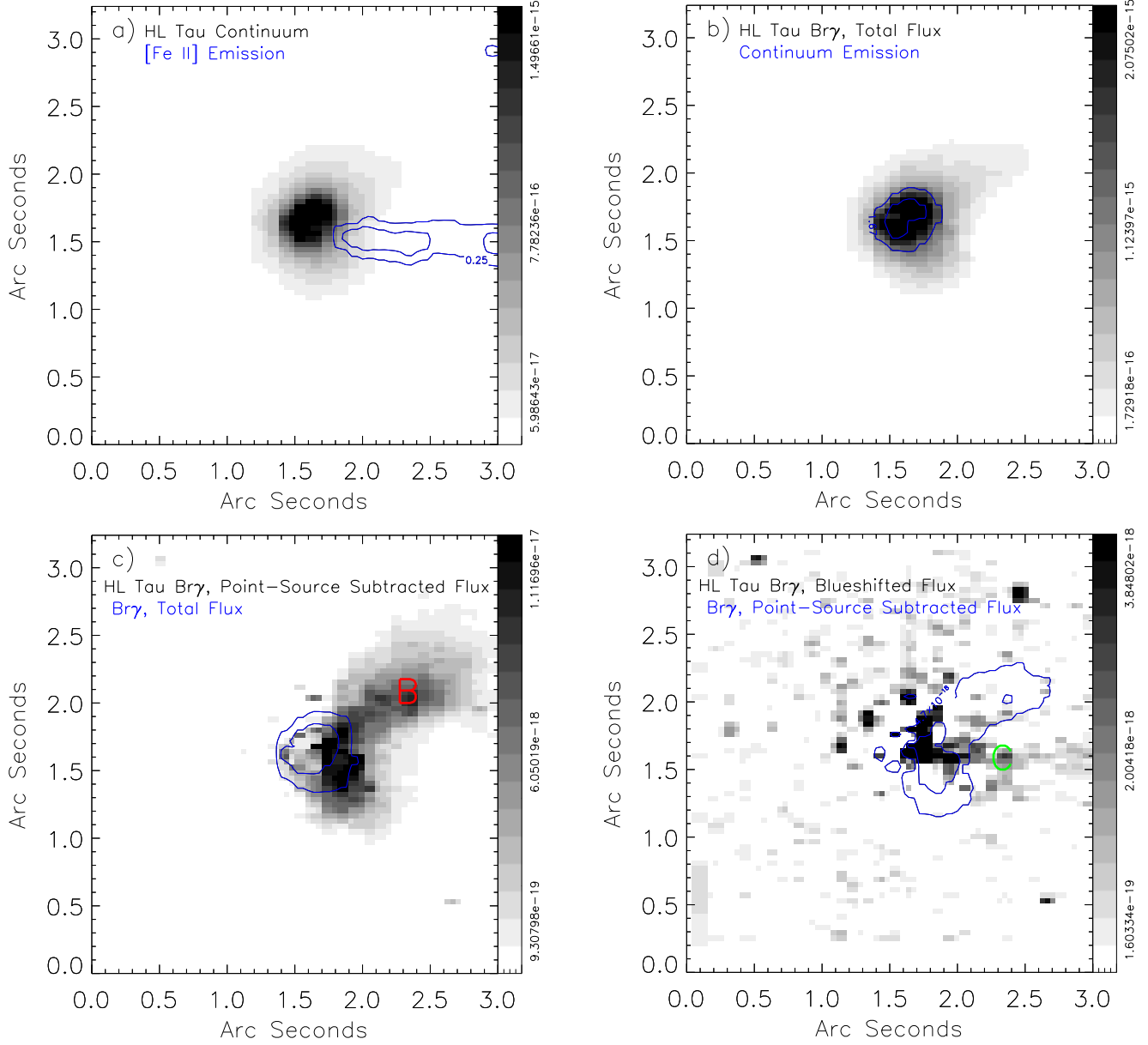


Fig. 3.— (a) The  $2.16\ \mu\text{m}$  continuum flux level from HL Tau with the  $0.''2$  occulting disk in the beam with contours of [Fe II] emission overplotted, designating the outflow location, (b) the continuum subtracted point-source Br $\gamma$  flux and (c) the continuum and (d) point-source subtracted map of spatially extended Br $\gamma$  from HL Tau. Also included here is a continuum and point-source subtracted map of spatially extended Br $\gamma$ , integrated over only two blue-shifted velocity channels (d). The (d) panel shows weak blue-shifted Br $\gamma$  emission that arises from the same spatial location as the [Fe II] emission from the outflow. The locations designated as "B" and "C" had 1-D spectral traces extracted, these are presented in Figure 5.

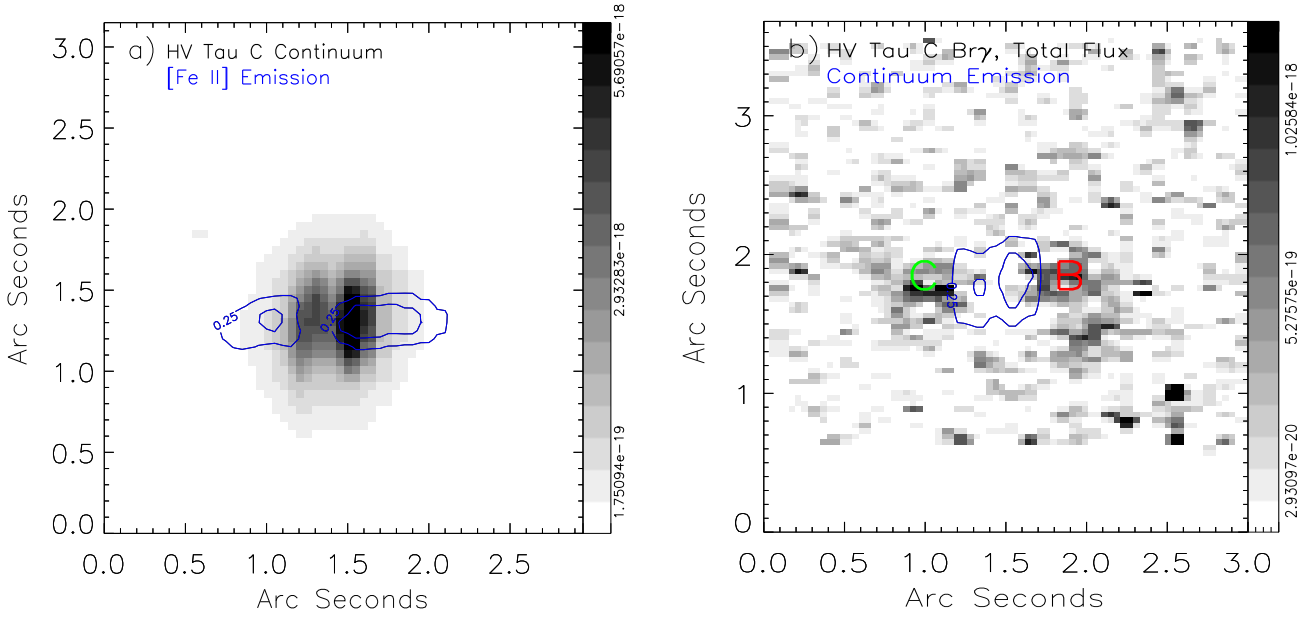


Fig. 4.— (a) The  $2.16 \mu\text{m}$  continuum flux level from HV Tau C with contours of [Fe II] emission overplotted, designating the outflow location, and (b) the continuum subtracted point-source Br $\gamma$  flux. The locations designated as "B" and "C" had 1-D spectral traces extracted, these are presented in Figure 5.



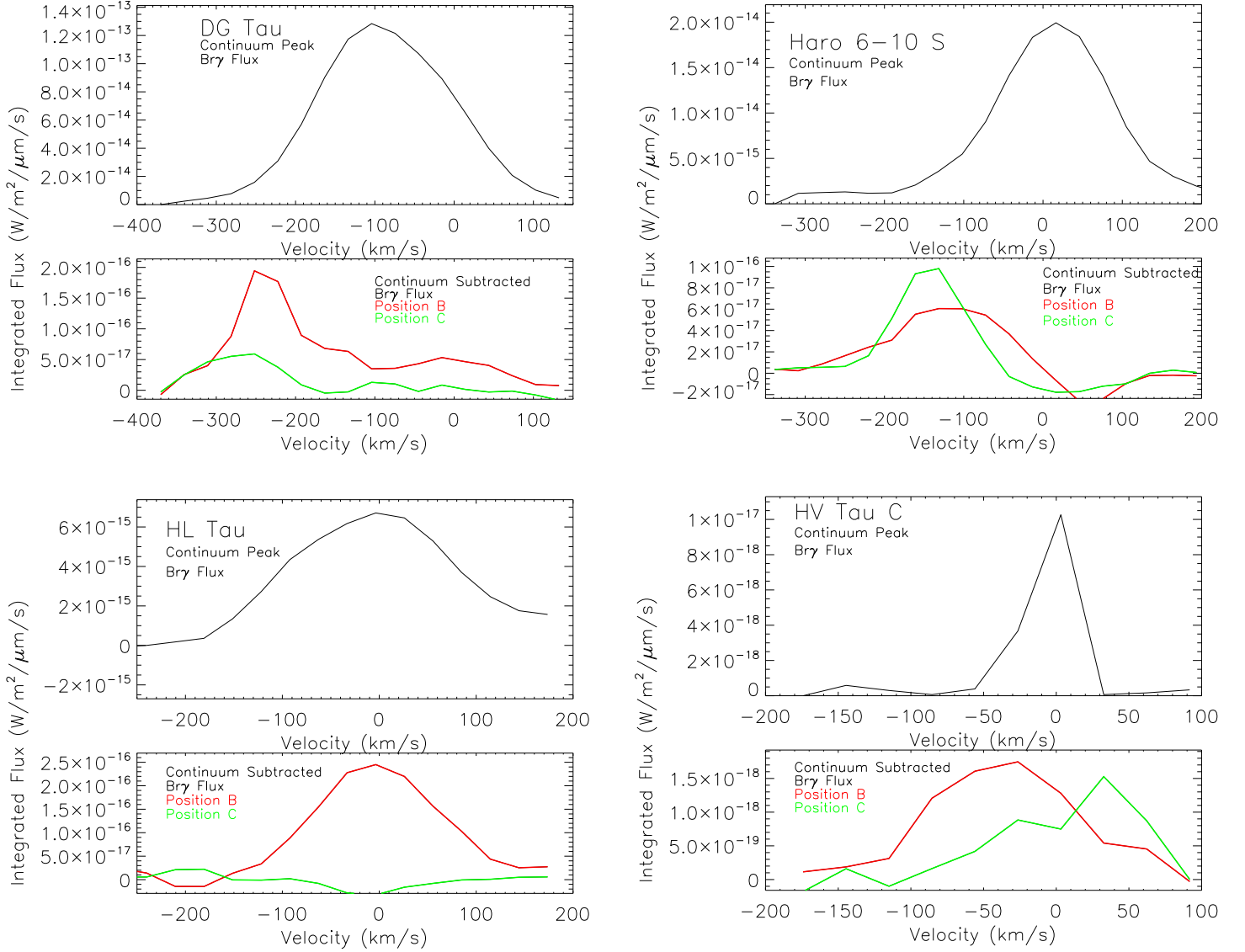


Fig. 5.— Br $\gamma$  flux versus velocity plots at the continuum peak locations and "Position B" and "Position C" (from plots 1-4) for DG Tau, Haro 6-10 S, HL Tau and HV Tau C. For DG Tau, HL Tau, and HV Tau C, the more spatially extended Br $\gamma$  emission measured at the "Position C" location is fainter and more blue-shifted than the less extended flux found at "Position B". For Haro 6-10 S, the "Position C" flux measures a bright knot in the Herbig-Haro flow and is stronger and more blue-shifted than the "Position B" emission.

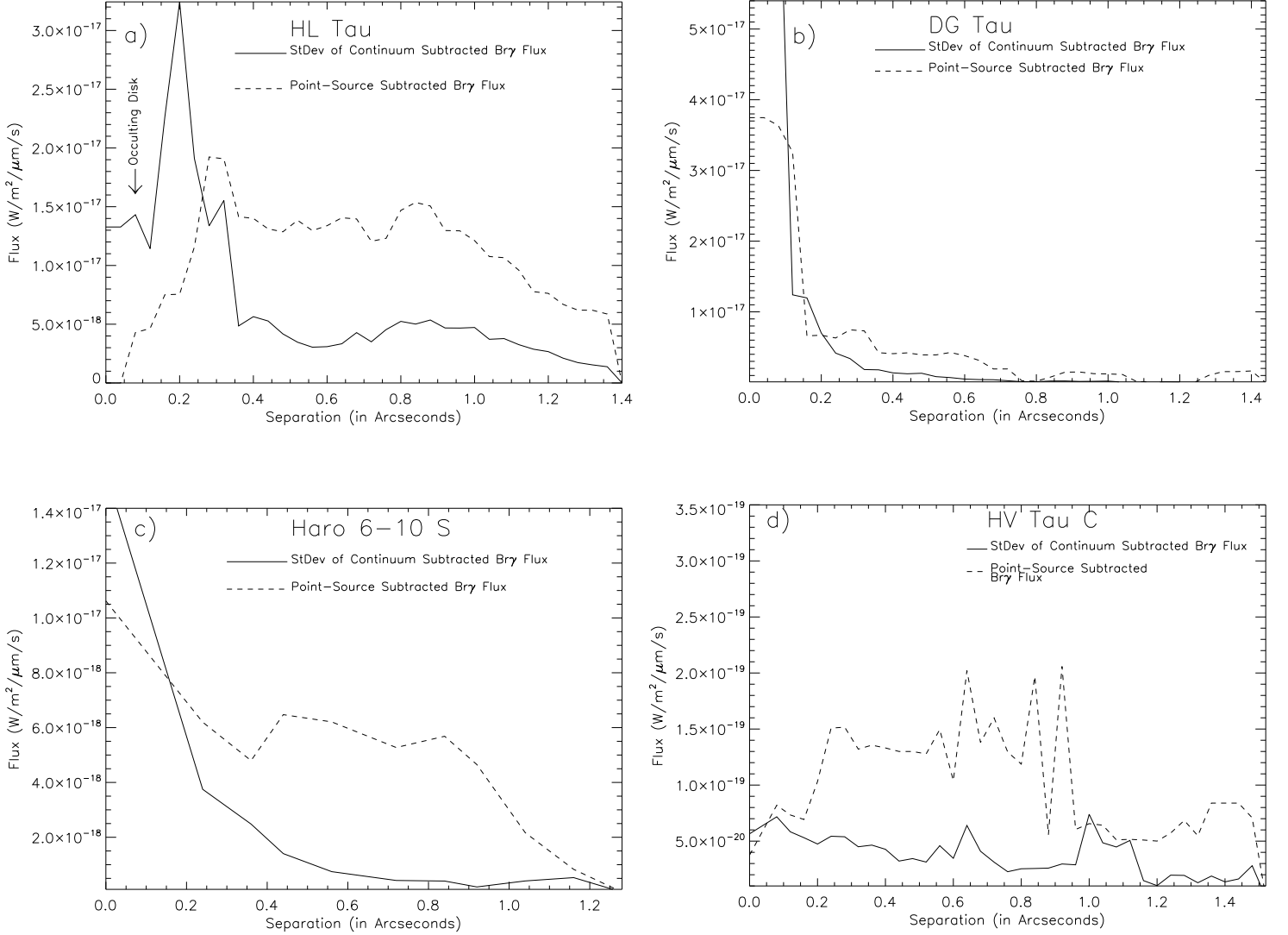


Fig. 6.— The standard deviation of the continuum subtracted Br $\gamma$  flux plotted versus distance from the central continuum peak for HL Tau (a), DG Tau (b), Haro 6-10 S (c) and HV Tau C (d). The overplotted dashed line represents the level of spatially extended continuum and point-source subtracted Br $\gamma$  flux. The ratio of the spatially extended flux to the standard deviation of point-source subtracted emission (dashed line to solid line) represents a measure of the signal-to-noise of the spatially extended Br $\gamma$ . The peak of the S/N for extended Br $\gamma$  is  $\sim 11$  for HL Tau,  $\sim 6$  for DG Tau,  $\sim 25$  for Haro 6-10 S, and  $\sim 11$  for HV Tau C.

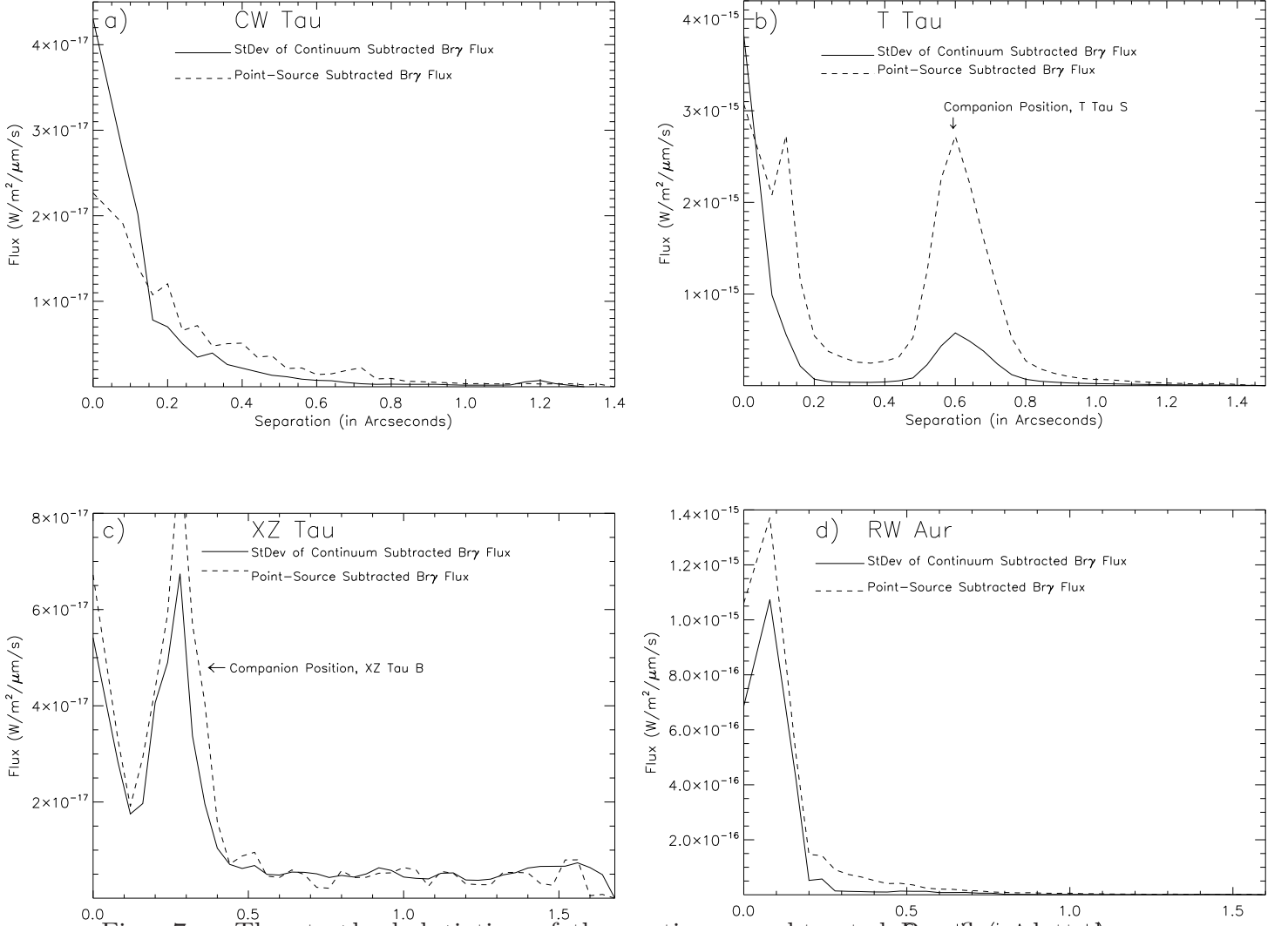


Fig. 7.— The standard deviation of the continuum subtracted  $\text{Br}\gamma$  flux plotted versus distance from the central continuum peak for CW Tau (a), T Tau (b), XZ Tau (c) and RW Aur (d). The overplotted dashed line shows the signal from point-source subtracted  $\text{Br}\gamma$  flux with increasing distance from the central star (e.g., XZ Tau A, RW Aur A, and T Tau N, in the case of the multiples). Flux peaks at  $0.''65$  and  $0.''25$  seen in T Tau and XZ Tau represent the positions of the stellar companions in these systems. The ratio of the dashed line to the solid line provides a measure of signal-to-noise in spatially extended  $\text{Br}\gamma$  flux, though the companions complicate the detection. It is clear from these plots that XZ Tau B and T Tau S have significant  $\text{Br}\gamma$  emission above their continuum flux. In these four cases, the S/N of spatially extended  $\text{Br}\gamma$  is less than  $\sim 3$  and there is no convincing evidence for spatially extended emission in any of these TTSs.